applied sciences

Article

Key Technologies for Longwall Cutting and Roof Cutting in Water-Infiltrated Soft Rock Tunnels of Shallow Coal Seams

Yitao Liu [1,2], Chong Li [1,3,*], Yadong Zheng [1,3,*], Yue Cao [1,3], Fan Zhang [1,3], Fan Qiao [1,3], Donglin Shi [1,3] and Mingxuan Wu [1,3]

[1] School of Mines, China University of Mining and Technology, Xuzhou 221116, China
[2] Ordos City Jintong Mining Industry Co., Ltd., Ordos 017000, China
[3] MOE Key Laboratory of Deep Coal Resource Mining, China University of Mining and Technology, Xuzhou 221116, China
* Correspondence: lichongky@163.com (C.L.); tb24020046a41@cumt.edu.cn (Y.Z.)

Abstract

This study addresses the major engineering challenges of leaving roadways along the goaf in shallow-buried coal seam tunnels through water-bearing soft rock. It focuses on three core issues: the mechanism of rock mass softening upon water exposure, large-deformation control, and directional pressure relief technology. By integrating laboratory testing, theoretical analysis, numerical simulation, and field testing methods, the evolution of macro- and micro-mechanical properties of rock under water–rock interaction can be studied. The research developed constant-resistance large-deformation rock bolts with "yielding within resistance and resisting within yielding" characteristics, revealed the mechanism of directional fracturing through shaped charge blasting, and proposed a synergistic control technology for along-the-goal rib retention: "shaped charge blasting for roof fracturing and pressure relief + reinforced rib support + debris retention devices." Research findings indicate: increased sandstone water content triggers dissolution of calcareous cement and expansion of clay minerals, leading to rock strength degradation and accelerated deformation, yet the failure mode remains uniaxial shear failure. The developed constant-resistance large-deformation anchor core device maintains a stable working resistance of approximately 350 kN within a 396–405 mm tensile deformation range, significantly enhancing the support system's crack-resistant capacity under pressure. The focused jet directs cracks to penetrate along predetermined paths, forming planar damage zones and effectively suppressing vertical damage to the surrounding rock. Based on field monitoring, the tunnel was divided into advance support zones, temporary support zones, and stable tunnel sections, enabling a differentiated support scheme. The engineering application achieved stable tunnel retention and safe reuse. This study provides key theoretical foundations and technical approaches for controlling rock mass stability in similar tunnel conditions.

Keywords: roof cutting; scanning electron microscopy; constant-resistance large-deformation anchor cables; shaped charge blasting; pressure relief

Check for updates

Academic Editor: Nikolaos K. Koukouzas

Received: 12 January 2026
Revised: 3 February 2026
Accepted: 4 February 2026
Published: 7 February 2026

1. Introduction

Top-cutting and pressure relief self-forming roadway technology, as an innovative pillar-less mining method, offers an effective solution to issues in traditional longwall mining, such as low resource recovery rates, high roadway maintenance costs, and the manifestation of strong dynamic pressure [1]. Its core concept involves actively intervening in the fracturing and displacement processes of the overlying strata. By utilizing the fragmented and expanded rock mass formed after roof rock failure and collapse to support the goaf, it automatically creates reusable roadways along the longwall sidewall, enabling safe, efficient, and environmentally sustainable continuous mining [1,2]. In recent years, as shallow resources have been depleted, coal mining has increasingly expanded into deeper, geologically complex conditions (such as extremely thin coal seams, thick hard roof strata, soft rock, and steeply dipping coal seams). This has placed higher demands on the adaptability, reliability, and precision control of roof cutting and pressure relief self-forming roadway technology [3–5].

Currently, scholars worldwide have conducted extensive research on roof cutting for self-forming roadways. In terms of technical principles and rock control mechanisms, it is generally recognized that creating artificial weak surfaces through roof cutting alters the structure of the overlying strata in the goaf, converting long cantilevers into short ones or achieving directional fracture of key layers, thereby optimizing the stress environment of the surrounding rock [6–8]. Successful roof cutting promotes timely caving and fragmentation of the roof strata. The collapsed debris supports the overlying strata, mitigating or even eliminating high abutment pressure at the working face, which is crucial for the long-term stability of self-forming roadways [9–11]. Technologically, two main methods have emerged: "Closely Spaced Drilling" (also known as Closed-Hole Roof Cutting) and "Pre-splitting Blasting." The former creates a weakened zone through dense boreholes. It is relatively safe and causes minimal disturbance to the surrounding rock, but its effectiveness depends heavily on parameter design [12–14]. The latter uses explosive energy for directional rock fracturing, offering high efficiency and broad applicability, especially under thick, hard roof conditions, though its impact on rock integrity and precision requires attention [15,16]. Research on applicable conditions has expanded from conventional medium-thick, horizontal coal seams to extreme conditions such as ultra-thin seams [17], thick-hard roofs [18], soft rock roadways [19], steeply dipping seams [20], and deep high-stress environments [21,22], with corresponding parameter optimization and control strategies proposed for different geological settings. Furthermore, methods like the N00 mining technique, which integrates bilateral roof cutting with self-forming roadways, have advanced the concept of pillarless mining [23,24].

However, applying roof cutting for self-forming roadways under complex geological conditions remains challenging. First, the precise design and dynamic adjustment of cutting parameters are critical. Different roof properties, thicknesses, and seam conditions impose specific requirements on cutting height, angle, and drilling/blasting parameters. Existing theoretical models and design methods still lack sufficient universality and precision [12,14,25]. Second, under challenging conditions such as strong dynamic pressure, deep high-stress zones, or composite roofs, controlling large deformations and ensuring long-term stability of self-forming roadways become prominent issues, necessitating integrated optimization of roof-cutting and high-strength support systems [26,27]. Moreover, in cases where thick, hard roofs resist timely caving, achieving directional, timely, and complete fracturing to release accumulated elastic energy is key to preventing dynamic hazards like rock bursts [18,28]. Additionally, existing research focuses primarily on roof control, with relatively less attention given to floor damage mechanisms and prevention, especially regarding water ingress issues [29].

In the current research, the primary challenges facing the roof-cutting and self-forming roadway technology can be summarized as follows: the precise design and dynamic control mechanisms for roof-cutting parameters under complex geological conditions remain unclear; achieving timely, directional fracturing of thick, hard roof strata and controlling energy release still pose difficulties; and existing studies predominantly focus on roof control while paying insufficient attention to the prevention and control of water-hazard-affected rock mass strength.

Under the directives for green and safe mining as well as the project's alignment with sustainable development goals, this study is conducted against the engineering background of self-forming roadways via roof cutting and pressure relief in shallow-buried thick coal seams. By integrating theoretical analysis, numerical simulation, and field testing, it systematically investigates the macro- and micro-scale evolution of water-bearing strata, the mechanical performance of novel constant-resistance large-deformation rock bolts, and the damage characteristics of blast-induced rock fracture. The research further proposes key technical parameters for the coordinated control of roof cutting and pressure relief coupled with high-resistance support. The outcomes aim to provide a theoretical foundation and technical reference for the safe, efficient, and sustainable application of roof-cutting self-forming roadway technology under similar geological conditions, thereby supporting the transition toward cleaner and safer mining practices.

2. Background

The 51,112 working face is located in the western section of Jintong Coal Mine. The 51,112 intake drift has a designed length of 660 m, as shown in Figure 1a. To the east lies the 51,113 working face, to the west the 51,111 working face, to the south the West Wing Rubber Conveyor Main Road, and to the north the 51,117 working face. The primary coal seam mined is the 5-1 seam, which exhibits stable occurrence. Its average burial depth is approximately 55 m, with thicknesses ranging from 0.94 m to 5.41 m and an average thickness of 2.86 m. The seam position is relatively stable, featuring predominantly simple structures, with well-developed coal seam bedding and joints. The roof strata consist of fine-grained sandstone, mudstone, and sandy mudstone, while the floor strata comprise siltstone and sandy mudstone. The lithology of the coal seam and its roof/floor strata is illustrated in Figure 1b. This is a low-gas mine. The working face is located in a low-lying area prone to water accumulation. Once the roof strata are affected by water, their strength weakens significantly.

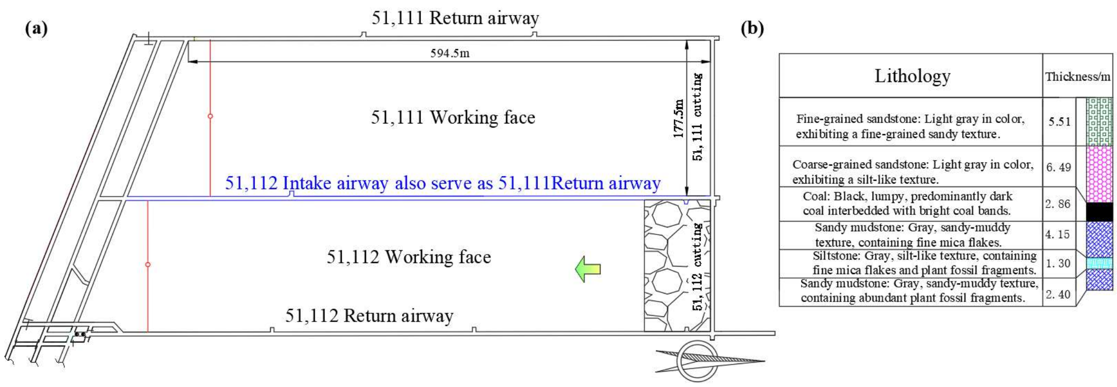

Figure 1. The 51,112 working face underground production geological conditions: (**a**) underground layout; (**b**) columnar diagram of the roof layer.

Based on borehole exposures documented in the Jintong Coal Mine exploration report and previous geological exploration findings, the strata sequence from oldest to youngest is as follows: Triassic Upper Series Yanchang Formation (T3y), Jurassic Middle-Lower Series Yan'an Formation (J1-2ya), Jurassic Middle Series Zhilo Formation (J2z), Quaternary Upper Pleistocene Series (Q3), and Holocene Series (Q4). The hydrogeological conditions are classified as a simple type dominated by pore and fracture recharge. Groundwater recharge and discharge flow from northwest to southeast. However, as mining operations expand and depths increase, particularly near drill holes where poor plugging quality causes hydraulic connectivity between aquifers, water inflow rates will correspondingly rise. Based on data provided by the mine, the measured normal water inflow rate for the 5-1 coal seam fully mechanized mining face is 192 m^3/d, with a maximum recorded inflow rate of 1560 m^3/d.

3. Materials and Methods

3.1. Materials

3.1.1. Specimens with Different Water Saturation Levels

To investigate the damage mechanics and rock failure characteristics of the direct roof sandy mudstone at Jintong Coal Mine under varying water saturation conditions, rock failure tests were conducted at different water saturation levels. Based on experimental requirements, water saturation test specimens (WSTCs) were prepared at 0%, 25%, 50%, 75%, and 100% (five specimens per group) saturation for uniaxial compression testing. To investigate the internal softening mechanism of specimens under water-saturated conditions, SEM scanning electron microscopy was performed on specimens with different water saturations. Changes in microstructure were analyzed to explain the softening mechanism of micro-minerals, pores, and fractures within the composite structure due to water.

3.1.2. Constant-Resistance Large-Deformation Cable Structure

Constant-resistance large-deformation rock bolts (cables) achieve a constant support resistance of 350 kN with maximum deformations reaching 1000 mm. The constant-resistance large-deformation anchor cable comprises a constant-resistance device, an anchor cable body, a support plate, and a nut. The constant-resistance device is fitted at the tail end of the anchor cable body (steel strand), with the support plate and nut sequentially mounted at the tail end of the constant-resistance device. The specific structure is shown in Figure 2.

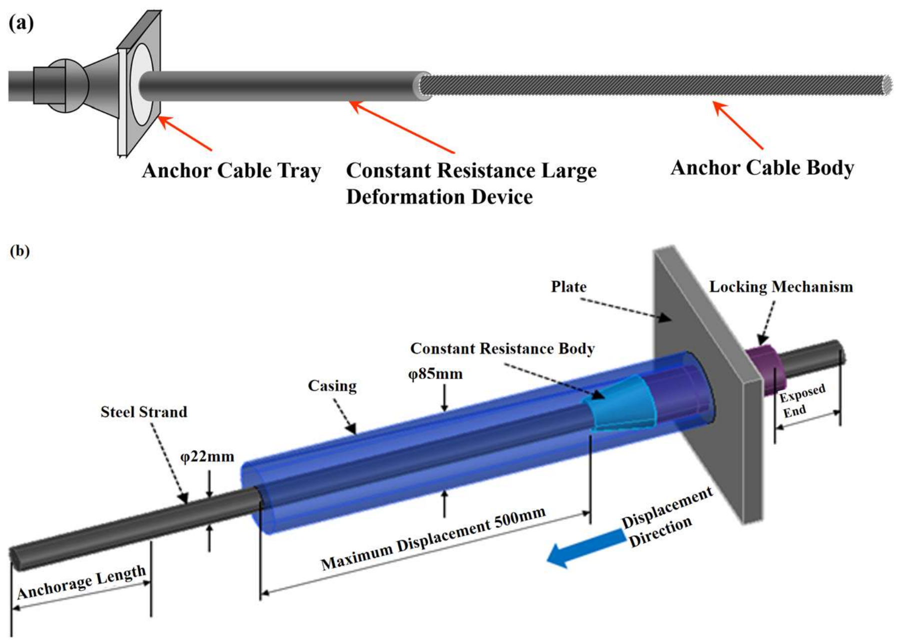

Figure 2. Schematic of constant-resistance large-deformation anchor cable structure: (**a**) schematic; (**b**) structural diagram.

3.2. Methods

3.2.1. Static Characteristic Testing of Constant-Resistance High-Deformation Anchor Cable

To evaluate the constant-resistance mechanical properties, constant-resistance value, and maximum static tensile elongation of the anchor cable while investigating its deformation characteristics, static tensile experiments were conducted. The horizontal tensile testing machine used was model LW-1000, comprising a mainframe, control cabinet, measurement and control system, and servo hydraulic power unit. The machine has a maximum test force capacity of 1000 kN, with a force measurement range of 2% to 100%. It provides a maximum tensile space of 4000 mm, and test results are controlled within a 1% error margin. Details are shown in Figure 3. Static tensile tests were performed on three constant-resistance large-deformation anchor cables: MS3-2-1, MS3-2-2, and MS3-2-3. Test data were recorded for each cable.

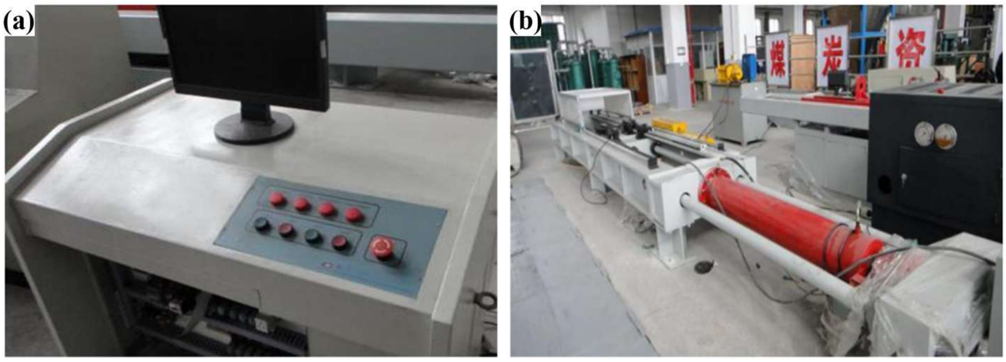

Figure 3. Horizontal tensile testing machine: (**a**) control cabinet; (**b**) tensile instrument.

3.2.2. Numerical Simulation of Directional Pre-Fracturing Energy-Concentrated Blasting

The LS-DYNA modeling in this study selected the RHT material type to simulate rock blasting, accounting for strain rate during compression and tension, strain hardening during material damage, and damage softening during compression. The strength criteria of the RHT model are expressed through three stress limit surfaces: the initial elastic yield surface, the failure surface, and the residual friction surface, which simulate blast-induced rock fracture. Within the RHT model, pressure is represented using the Mie–Greisen form, employing a polynomial Hugoniot curve and a p-α compaction relationship. This model enables precise prediction of crack initiation and propagation in rock under dynamic loading [11,12].

This study primarily investigates rock damage and failure under combined stress and shaped charge blasting effects. Therefore, the model is developed based on actual shaped charge blasting engineering practices. The shaped charge blasting employs shaped charge tubes loaded with explosives. The drill hole spacing is 500 mm, the shaped charge tube length is 1500 mm, the inner diameter is 38 mm, and the outer diameter is 46 mm. The explosive used is a secondary emulsion explosive with dimensions of $\Phi 32 \times 300$ mm. During blasting, two explosive charges are installed in each shaped charge tube. The computational model replicates the actual project with a 1000 mm cube. A 50 mm diameter borehole is drilled at the model's center, reaching 800 mm depth. The explosive length matches the shaped charge tube at 600 mm, with a 200 mm sealing clay section. The air chamber dimensions are $500 \times 500 \times 1000$ mm^3. The shaped charge blasting computational model is shown in Figure 4. In subsequent modeling, the explosive was ignited at its center.

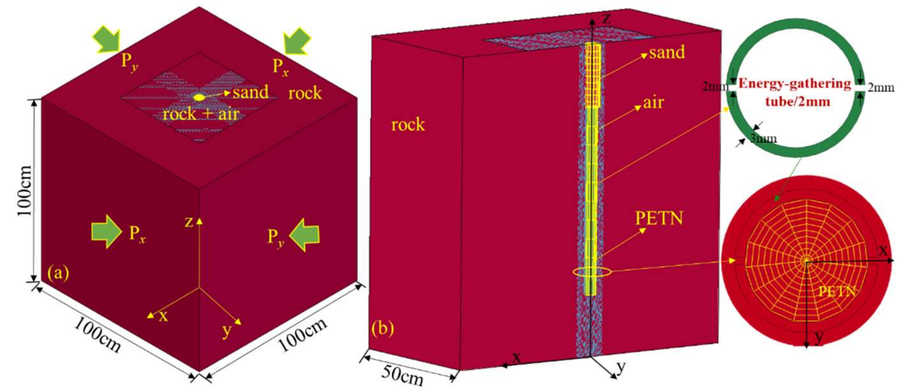

Figure 4. Modeling of concentrated-energy blasting.

3.2.3. Force Analysis of Constant-Resistance Large-Deformation Anchor Cables

This study employs a combined approach of qualitative analysis based on mechanical principles, simplified construction of fundamental physical models, and validation of key material parameters. Engineering deployment diagrams identified the critical support positions of constant-resistance large-deformation rock bolts in the roof of the goaf on the working face side. The support mechanism was systematically explained: enhancing roof bending resistance to suppress delamination and rotation, absorbing energy through large-deformation characteristics to mitigate blast impacts, and preventing sudden failure via the constant-resistance mechanism. Based on the structural schematic diagram, a simplified cylindrical mechanical model of the core friction assembly was established. The force equilibrium equations were derived using the principle of limit equilibrium, emphasizing key design criteria for achieving stable, constant-resistance performance through pre-engineered friction pairs and optimized creep [3,9,13,18].

4. Results and Analysis

4.1. Changes in Mechanical Properties and Failure Characteristics of WSTCs

Figure 5a demonstrates a negative correlation between the water saturation of the coal–rock composite and its uniaxial compressive strength. The uniaxial compression process exhibited typical stages of compaction, linear elasticity, yield, and failure. At 0% water saturation, the maximum uniaxial compressive strength reached 19.95 MPa. This strength progressively decreased to 14.60 MPa at 25% saturation, 10.86 MPa at 50% saturation, 4.51 MPa at 75% saturation, and a minimum of only 2.06 MPa at full saturation (100%).

It is widely recognized that the strength of rock specimens is governed by the initiation and propagation of cracks during loading. Figure 5b illustrates the corresponding failure modes of the coal–rock assemblies under uniaxial compression at different saturation levels. Due to the presence of angled bedding planes in the sandstone, failure primarily manifested as monoclinic shear. At 0% saturation, failure resulted in a single fracture plane. As water saturation increased to 25%, the failure released substantial energy, forming two primary fracture planes that propagated downward and interconnected within the coal matrix, resulting in a tensile–shear failure mode. At 50% saturation, conjugate-plane shear failure was observed. At 75% and 100% saturation, the specimens failed via single-plane shear. Analysis of the uniaxial stress–strain curves indicates that while water content does not alter the fundamental type of crack propagation, it significantly accelerates the rate of rock failure.

Microstructural analysis (Figure 5b) provides further insight into the water–rock interaction mechanism. In the dry state (0% moisture), mineral surfaces appeared smooth with grains tightly bound by cementation material, and pores/cracks were relatively distinct. With increasing moisture content, dissolution of calcareous cement occurred, leading to the development and interconnection of micro-pores and micro-cracks. Clay minerals exhibited noticeable swelling, resulting in grain loosening. At saturation, the microstructure transitioned from a dense, pore-cemented fabric to an irregular, honeycomb-like structure. This evolution featured fewer particles on pore walls, the closure of some micro-pores, and the development of larger, better-connected pores. Macroscopically, these changes correspond to the observed strength deterioration and increased deformation.

The combined macro- and micro-scale evidence confirms that the water-induced softening of rock is fundamentally a process of cumulative structural damage driven by physicochemical interactions [30,31].

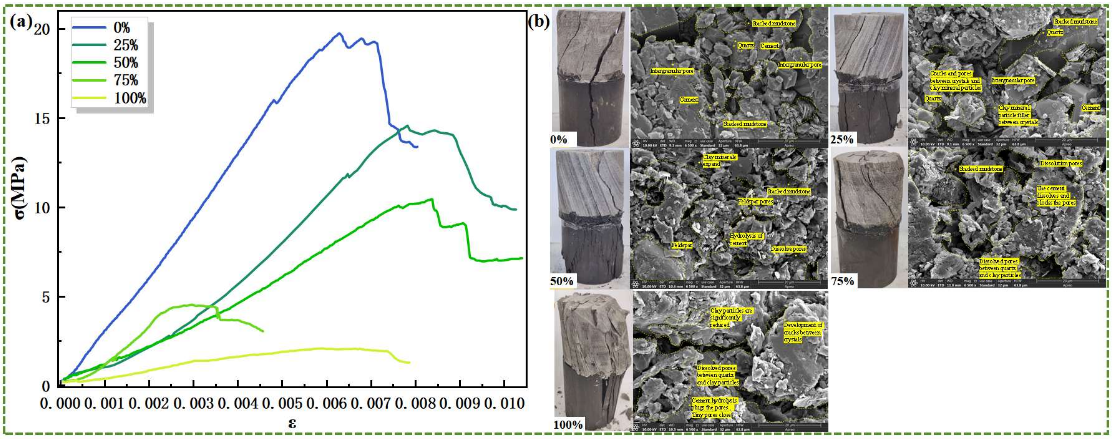

Figure 5. Mechanical properties and microstructural changes diagram: (**a**) stress–strain curve; (**b**) failure mode of coal–rock assembly and SEM test results.

4.2. Constant-Resistance Anchor Cable Support Technology

4.2.1. Mechanism of Constant-Resistance Large-Deformation Anchor Cable Support

Traditional prestressed anchor cables exhibit low elongation, rendering them unsuitable for accommodating the large-deformation failure characteristics of surrounding rock in underground engineering. When significant deformation occurs, the initial deformation energy exceeds the reserve capacity of the anchor rod, causing failure of the prestressed anchor cable support system. A key distinction between constant-resistance large-deformation anchors (cables) and conventional prestressed anchors lies in their "yielding with resistance, resisting with yielding, and preventing breakage while maintaining constant resistance" characteristic. A core component enabling this feature is the design of a novel constant-resistance device. Integrating this device into traditional prestressed anchors achieves constant-resistance large-deformation functionality. This addresses the limitations of conventional prestressed anchorage systems, such as low elongation rates that fail to accommodate significant rock mass deformation.

4.2.2. Working Principle of Constant-Resistance High-Deformation Anchors (Cables) for Rock Mass Pressure Control

(a) Pre-deformation stage—Installation of new anchor cables

After excavation of underground structures, the originally stable rock mass is disrupted. On one hand, stress redistribution leads to stress concentration where the rock's inherent mechanical properties cannot withstand the load, creating plastic zones or tension zones. On the other hand, construction induces rock mass relaxation, compounded by geological structures, reducing overall stability. Therefore, before significant deformation or failure occurs, constant-resistance large-deformation anchor rods (cables) must be installed according to the underground engineering support design requirements, using traditional prestressed anchor cable construction techniques.

(b) During Rock Mass Deformation—Absorbing Deformation Energy

During the initial stage of large-deformation failure in underground engineering rock mass, the energy is substantial. When the deformation energy exceeds the constant-resistance range of the anchor cable, the constant-resistance body slips within the constant-resistance sleeve. This means the constant-resistance large-deformation anchor rod (cable) undergoes large radial stretching deformation in response to the rock mass's large deformation, thereby absorbing deformation energy and preventing anchor cable failure or rupture caused by significant rock mass deformation.

(c) Post-Rock Mass Deformation—Tunnel Stability

After the surrounding rock undergoes large deformation, the internal stress within the rock mass reaches a new equilibrium, releasing its stored energy. The deformation energy of the surrounding rock becomes less than the designed constant-resistance T of the constant-resistance device. The axial force P of the anchor cable is less than the frictional resistance between the constant-resistance device and the constant-resistance sleeve. With the support of the constant resistance of the large-deformation anchor rod (cable), the surrounding rock returns to a stable state. Details are shown in Figure 6.

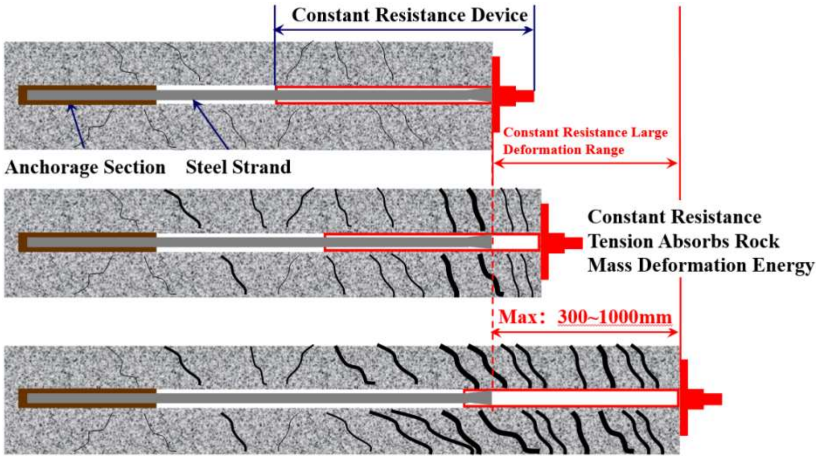

Figure 6. Support the principle of constant-resistance large-deformation anchor bolts (cables).

4.2.3. Mechanical Characteristics of Constant-Resistance Large-Deformation Cable

Static tensile test results (Table 1) indicate: under tensile force, the working resistance of the constant-resistance large-deformation cable rises rapidly, representing the elastic resistance increase phase. Once the working resistance reaches a certain level, the constant-resistance device begins to slip and deform, entering a state of essentially constant resistance—the constant-resistance deformation phase. The elongation of constant-resistance large-deformation anchor cables ranges from 396 to 405 mm. During tensile deformation, the working resistance remains stable at approximately 350 kN, meeting design requirements. Details are shown in Figure 7.

Table 1. Static tensile test data for constant-resistance large-deformation anchor cables.

No.	Specimen Length (mm)	Constant-Resistance Device Length (mm)	Final Elongation (mm)	Constant-Resistance Range (kN)	Remarks
MS3-2-1	1502	400	405	349–359	Pulled out
MS3-2-2	1500	400	399	319–340	Pulled out
MS3-2-3	1503	400	396	308–359	Pulled out

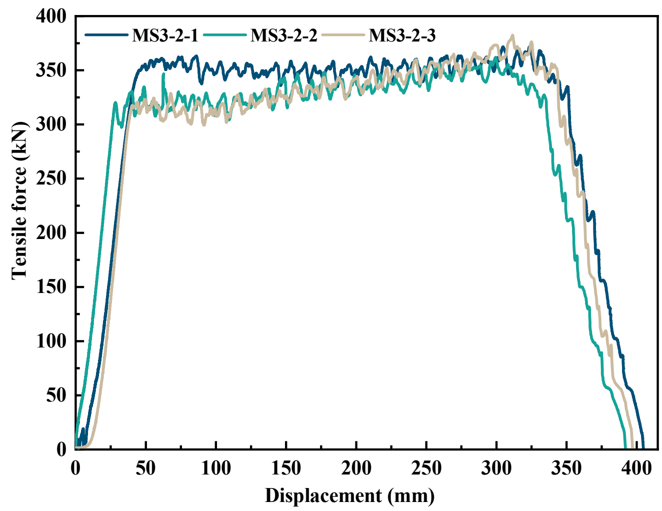

Figure 7. Static tension test curve for constant-resistance large-deformation anchor cable.

4.2.4. Key Support Areas for Constant-Resistance Large-Deformation Anchor Cables

The roof of the goaf adjacent to the longwall face represents a critical failure zone for roadway deformation. Before longwall mining, constant-resistance large-deformation anchor cables were deployed to reinforce this goaf roof section, as illustrated in Figure 8.

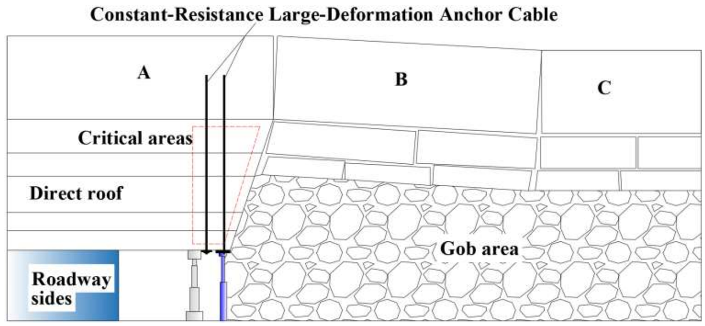

Figure 8. Position of constant-resistance large-deformation anchor cable support.

Reinforcing the side roof of the goaf with constant-resistance large-deformation anchors enhances the bending moment resistance capacity of the roof strata on the solid coal side. This effectively prevents roof separation and displacement; the increased bending moment resistance of the roof rock layer limits the rotation of the main roof toward the goaf, reducing the compressive force exerted by the main roof on the goaf side's immediate roof. This prevents the crushing and fragmentation of the immediate roof rock mass on the goaf side, thereby avoiding roof collapse and leakage. Resisting the blasting impact disturbance from pre-splitting blasting on the side roof of the goaf, absorbing blasting energy, ensuring the integrity and stability of critical roof sections, thereby preventing structural failure and achieving the objective of stabilizing the surrounding rock in deep roof cutting and pressure relief with roadway retention along the goaf. Constant-resistance large-deformation rock bolts (cables) maintain resistance even when axial force exceeds constant resistance, preventing sudden failure and surrounding rock destruction. In underground engineering projects utilizing this novel anchor cable as support material, when the surrounding rock undergoes deformation, the cable stretches accordingly to release deformation energy. Even after elongation, the cable maintains constant working resistance, stabilizing the surrounding rock and eliminating safety hazards such as roof falls, cave-ins, rib buckling, and severe floor heaving. The structural diagram of the constant-resistance device is shown in Figure 9.

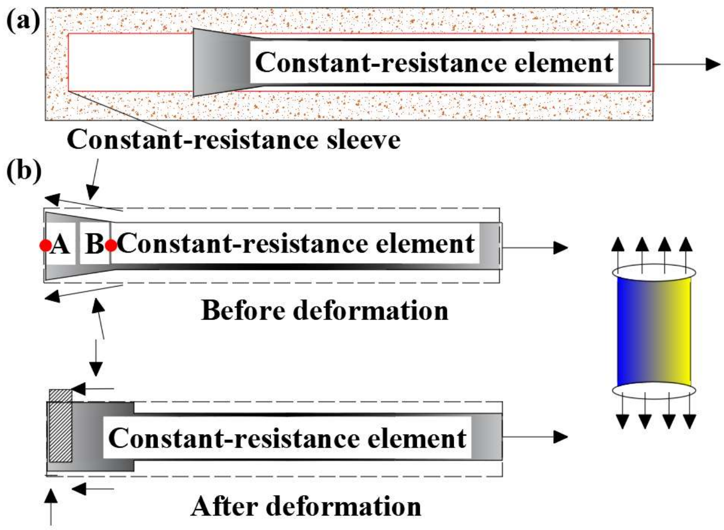

Figure 9. Mechanical model of constant-resistance device support: (**a**) schematic diagram; (**b**) mechanical model.

Based on the working principle of a constant-resistance large-deformation anchor rod (cable) support, prior to installing the new anchor cable, drill holes at appropriate locations according to the design plan. Then insert the constant-resistance large-deformation anchor rod (cable) into the drilled holes. Inject cement mortar or resin grout between the constant-resistance device and the drilled hole to tightly bond the constant-resistance device with the surrounding rock, forming the anchoring segment. The constant-resistance function is achieved through pre-designed friction between the constant-resistance body and the constant-resistance casing. Since the stability of constant-resistance directly impacts the overall performance of the constant-resistance large-deformation anchor rod (cable), the selection of the constant-resistance body, constant-resistance casing, and new constant-resistance filling material is critical. It is essential to maximize the mitigation of material creep and relaxation. When calculating shear stress at the contact surface between the constant-resistance body and sleeve, the calculation originates from the base of the frustum (Point A) and extends to its apex (Point B).

Since the radii of the upper and lower bases of the constant-resistance body's frustum are nearly identical, it can be simplified as a cylinder. Based on this simplified mechanical model, select a differential segment dz on the cylinder. Let τ denote the shear stress around this segment. Considering the minimal contact area between the cylinder and the constant-resistance sleeve, stress distribution across this cross-section is approximated as uniform. The stress at the cross-section is σ, and the stress at the $z + dz$ cross-section is σ-$d\sigma$. Assuming the radius of the cylindrical cross-section is R, the principle of limit equilibrium yields:

$$Rdz = -2\tau dz \tag{1}$$

Therefore, the shear stress around the differential segment can be expressed as:

$$\tau = -\frac{R}{2} \cdot \frac{d\sigma}{dz} \tag{2}$$

The derivation process of Equation (3) is referenced in Appendix A. Comprehensive Equation (A1) to Equation (A5):

$$\varepsilon = \frac{\sigma}{E} = \frac{N}{E \cdot S} \tag{3}$$

https://doi.org/10.3390/app16041678

The physical meaning of Equation (3) is: when the constant-resistance large-deformation anchor rod (cable) reaches ultimate mechanical equilibrium, i.e., when the axial force equals the constant-resistance force, the strain incurred by the constant-resistance body's conical head provides 350 kN of constant-resistance force.

4.3. Blasting Cutting Simulation Analysis

To balance computational accuracy and time, after mesh convergence testing, a 10 mm cubic element was used for modeling. The model employed fluid–structure interaction simulation, where air shared nodes with rock, explosives, shaped charge tubes, and plugging materials. Testing utilized the same algorithm as the model validation. The simulation concluded when existing cracks ceased propagation and no new cracks formed, with a simulation duration of 1000 μs. Shaped charge blasting plays a crucial role in both mining and tunnel excavation. To investigate rock mass damage and crack development under uniaxial stress during shaped charge blasting, research was conducted based on prior studies of loosening blasting. Explosives are placed inside the shaped charge tube, which is designed as a tubular structure using specific materials. Shaping grooves are positioned on both sides of the tube to form the shaped charge. When explosive energy is released, these grooves concentrate the energy, directing the explosion stress wave to propagate along the tube's axis. The shaping grooves are oriented parallel to the x-direction. The results are shown in Figure 10.

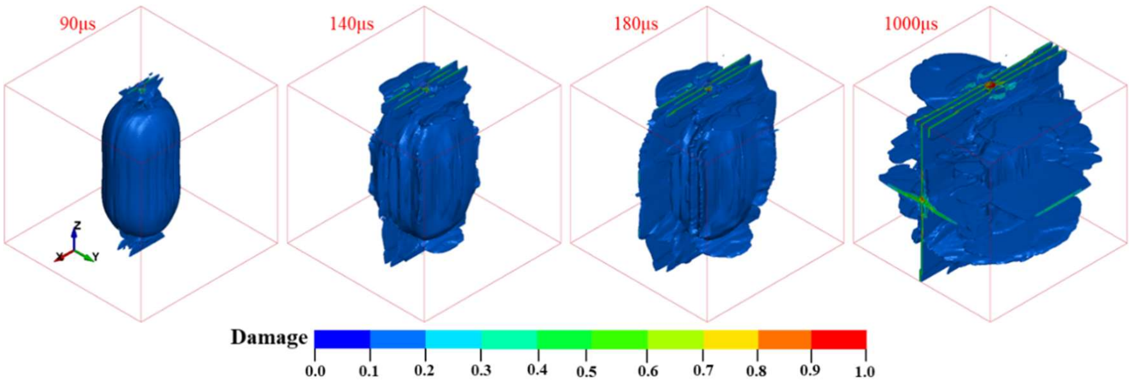

Figure 10. Stress wave attenuation.

Upon initiation of the blasting sequence, an ellipsoidal stress wave first forms around the explosives. This wave induces intense compression on the shaped charge tube, creating a fragmentation zone near the tube and generating concentrated tensile stress along the shaping direction. When the explosive stress radiates to the surface of the shaped charge, part of the energy forms a shaped jet along the direction of energy concentration. In the non-concentration direction, the stress wave reflects, and the reflected stress wave ultimately radiates along the direction of energy concentration. The gas jet contacts the surrounding pressure, partially compressing the rock. When the pressure generated by the explosive stress wave exceeds the rock's compressive strength, tensile cracks form in the surrounding rock. The stress wave primarily radiates along the uniaxial stress direction, while stress waves perpendicular to the stress direction are suppressed. As shown in Figure 11, damage parallel to the focusing direction is fully penetrated, while damage perpendicular to the focusing direction is only about 50 mm. Figure 12 indicates that cracks primarily develop along the focusing direction. The damage level inside the model gradually decreases, and the damage area progressively forms a surface. This effectively protects the integrity of the surrounding rock, achieving the effect of focused cutting.

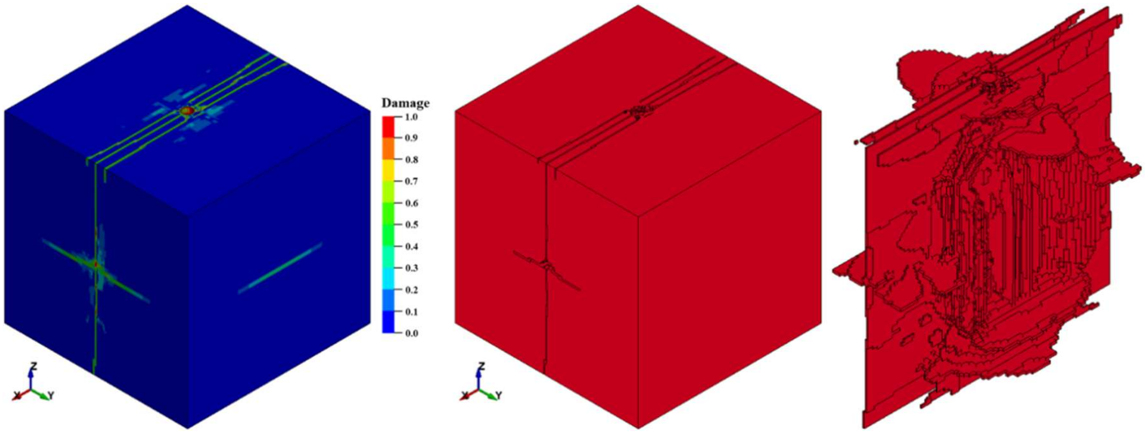

Figure 11. Crack evolution.

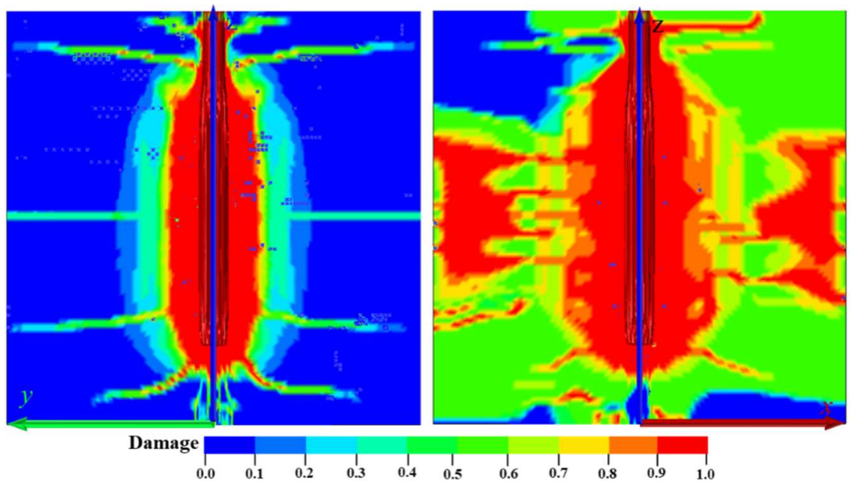

Figure 12. Damage contour map.

5. Gob-Side Entry Retaining Plan and Monitoring

5.1. Blasting Roof Cutting and Pressure Relief Plan

Bidirectional energy-focusing tubes utilize specially manufactured tubes. These tubes feature an outer diameter of 42 mm, an inner diameter of 36.5 mm, and a length of 1500 mm. The focused blasting employs Grade II emulsion explosives for coal mines, with the proposed charge specifications being Φ32 mm × 300 mm per roll. During field trials, the focused charge tubes are installed within the blast holes. Based on field trial results, the charge structure and quantity are adjusted on time. The blast hole openings are sealed with gunning paste using specialized equipment. During field trials, the blasting structure and method must be determined and adjusted based on the rock properties of the roof, as confirmed through prior working face mining conditions. Shotcords were installed within the blast holes, with charge configuration and quantity adjusted promptly based on field test results. The blast hole openings were sealed using specialized equipment and shotcrete. The roof of the 51,112 intake drift is classified as weak. Tests were conducted specifically for this condition, and post-blast inspections of the drilled holes were performed using an intrinsically safe borehole imaging device. Based on field test results, the optimal charge configuration for the hard roof section is 2-2-1-1 (6 rounds), with a hole spacing of 550 mm, four shaped charge tubes per hole, and an optimal sealing clay length of 3 m. Details are shown in Figure 13.

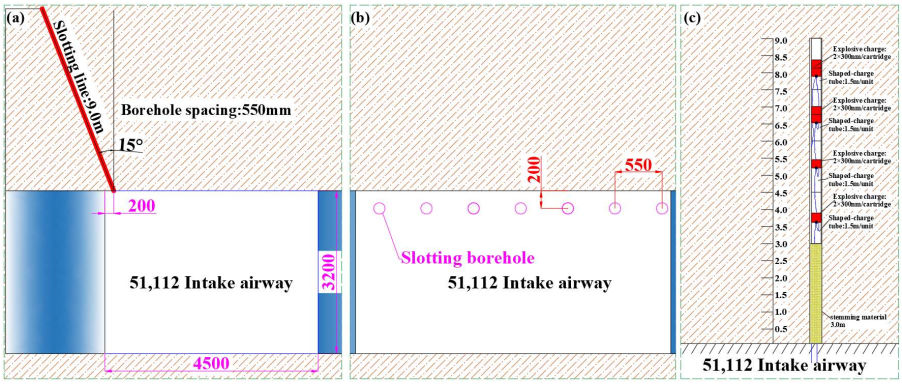

Figure 13. Slot drilling design diagram: (**a**) cross-section; (**b**) plan view; (**c**) slot charging parameters.

5.2. Support Scheme for Leaving Galleries Along the Goaf

During face advancement, galleries at different locations experience varying degrees of mining-induced deformation. The advanced section of the face is subjected to advanced pressure. After face extraction, the roof begins to collapse, and a certain period is required for the collapse to stabilize. During this interval, the gallery is affected by dynamic pressures such as fracturing stresses and collapse impacts. Therefore, the area behind the supports near the working face requires not only roof support but also rock-blocking support. As the working face advances further, when the roadway is farther from the face, roof movement generally stabilizes. At this point, the equipment used for temporary support behind the supports can be removed, and only rock-blocking support is necessary. Based on historical field monitoring data, the roadway near the working face is divided into three zones: advance support zone, temporary support zone behind the roof, and stable roadway zone. The temporary support zone behind the roof is designed to be 130 m to 150 m long according to site conditions and engineering experience, with the actual length determined by mine pressure monitoring results. Different support measures are adopted for each zone as needed, with the zoning shown in Figure 14.

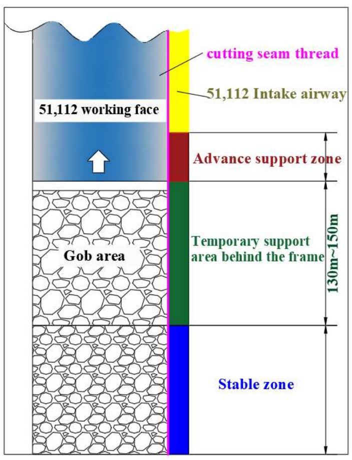

Figure 14. Design zoning diagram for temporary tunnel support.

5.2.1. Temporary Support Area Behind the Frame

This roadway segment lies within the advanced influence zone of the working face. Rock falls from the goaf roof exert frictional forces on the roadway roof, subjecting it to significant dynamic pressure with high roof stress. Consequently, temporary reinforcement is required for the roof. Based on engineering experience and site conditions, the temporary support distance within the roadway is preliminarily set at 130 m to 150 m, with the actual distance determined by roadway rock pressure monitoring data. The proposed design solution is as follows [18,20]:

The roadway roof shall be supported using a "single hydraulic prop + π-shaped steel beam + unit support" configuration. Unit supports shall be installed at 2.4 m intervals, totaling 63 units. Each unit support shall be equipped with two single props and a π-shaped steel beam, with a row spacing of 1 m. The roadway cross-section design calls for single-row single props (DWX35/4.0-300), which must be fitted with shoe plates and caps. Once the surrounding rock stress and deformation in the retained roadway stabilize, the temporary single pillars and π-shaped steel beams can be progressively removed. After removal, the roadway roof will primarily rely on constant-resistance rock bolts for support. The temporary roof support design is illustrated in Figure 15.

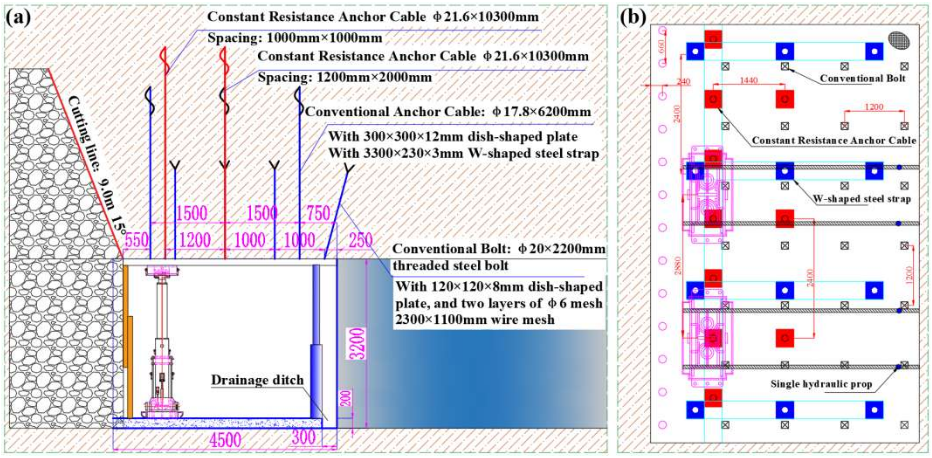

Figure 15. Temporary support for longwall mining: (**a**) cross-section; (**b**) plan view.

5.2.2. Stable Zone

"Dense Single-Pillar" technique along the tunnel: immediately after face extraction, arrange one or more rows of densely spaced single pillars along the blasted pre-split line. The upper ends of the pillars are connected to the roof using wooden blocks as a flexible cushion layer. Individual props offer rapid resistance increase and high stiffness, promptly providing substantial roof-cutting resistance. This facilitates controlled roof collapse along the pre-split line in the goaf while simultaneously supporting the roadway roof, preventing rapid subsidence during the initial roadway retention phase. Single pillars near the cutting seam are supplemented with I-beams and metal mesh for rock support. I-beams are spaced between pillars, while metal mesh is securely fastened to I-beams with wire ties. After the working face advances, this effectively prevents waste rock from the goaf from flooding into the roadway, achieving excellent rib formation. After the roof in the goaf fully collapsed and compacted, the single pillars could be gradually withdrawn. The side walls of the goaf side road were then sprayed with concrete to seal the goaf and isolate harmful gases.

During actual application, it was found that the limited space at the 51,112 working face cut-off section precluded the use of unit supports. Therefore, a "single hydraulic prop + π-shaped steel beam" configuration—substituting a single beam with four props for unit support—was employed for approximately 10 m of the cut-off section. Additionally, after advancing 100 m, the supply of unit support temporarily could not keep pace with the mining speed. Therefore, it is planned to replace the original support configuration with "single hydraulic props + π-shaped steel beams." Once unit supports are regularly supplied, the original support design "single hydraulic props + π-shaped steel beams + unit supports" will be reinstated for roadway roof support.

The support design is as follows: employ "single hydraulic props + π-shaped steel beams" for roadway roof support, with a row spacing of 0.8 m. The roadway cross-section design utilizes single-row single props (DWX35/4.0-300), which must be fitted with shoe plates and caps. Temporary support beyond the 130–150 m range after tunnel framing may be determined based on monitoring results. Once the surrounding rock stress and deformation in the retained tunnel section stabilize, temporary support components (individual pillars and π-shaped steel beams) within the tunnel may be progressively withdrawn. After complete withdrawal, the roof of the retained roadway is primarily supported by constant-resistance rock bolts and similar measures. For roadway rib support: employ retractable 29U-shaped steel beams combined with steel mesh reinforcement, arranged along the cutting line at 800 mm intervals. Adjacent retractable U-shaped steel beams are connected using clamping cables and connecting rods. The temporary roof support design is illustrated in Figure 16.

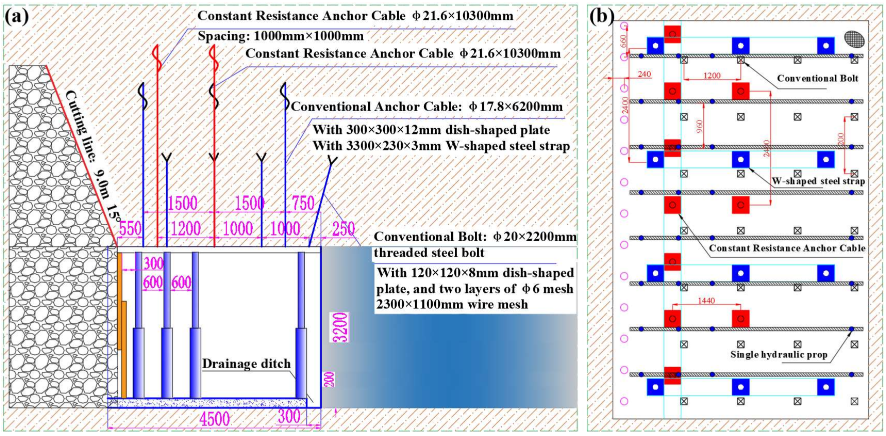

Figure 16. Temporary support for roadway retention along goaf (single pillar): (**a**) cross-section; (**b**) plan view.

The reinforcement mesh consists of welded steel mesh with 6.0 mm diameter bars, sized 2600 mm × 1100 mm. Each mesh panel overlaps adjacent panels by 100 mm and is secured with galvanized iron wire (No. 14). The mesh overlaps with the existing metal mesh support. A ventilation duct fabric is hung behind the mesh to prevent air leakage. For severe debris leakage, diamond-shaped metal mesh can be added inside the reinforcement mesh to enhance debris containment support.

5.2.3. Construction Process of Constant-Resistance Large-Deformation Anchor Cables

The construction of constant-resistance large-deformation anchor cables is shown in Figure 17. The construction process is as follows: conduct constant-resistance anchor cable reinforcement support construction according to design requirements. First, rigorously inspect the roadway cross-section dimensions against the centerline and waistline. Any deviations from the work procedure requirements must be addressed before proceeding. Before drilling, conduct a rock-wall inspection to carefully assess the condition of the roof and sidewall rock mass, removing loose debris and unstable rocks. Work may only commence after confirming safety. Anchor cable positioning must be precise, with hole location errors not exceeding 100 mm and hole orientation errors not exceeding 2°. The process flow is: Tap the sides and top → Determine hole positions → Prepare drilling tools → Mark anchor holes → Drill anchor holes → Enlarge constant-resistance device installation holes → Install grout and steel strands → Thoroughly mix grout to anchor cables → Install W-shaped steel bands → Install anchor trays → Install constant-resistance devices → Install locking devices → Apply pre-tension → Clean the site.

Figure 17. Construction process of constant-resistance anchor cable.

Integrating research findings, the following parameters were determined: roof cutting and pressure relief scheme, length of temporary support behind roof supports, and enhanced support scheme parameters. These improvements enhance the stability and safety of longwall roadways.

5.3. Mine Pressure Monitoring Plan During Roadway Retention

5.3.1. Monitoring Content

Monitoring points shall be established primarily to track the stress and deformation of constant-resistance anchor cables and temporary single pillars within the roadway, while also monitoring asymmetric deformation on the roadway rock surface. Starting from the tunnel retention point—within the first 150 m—install one monitoring station every 20 m, totaling 7 stations. Each station must simultaneously house: constant-resistance cable stress monitoring equipment—hydraulic single-column stress monitoring equipment—unit support stress monitoring equipment—shrinkage monitoring equipment—tunnel surface asymmetric deformation observation points. Beyond 150 m: install one monitoring station every 50 m, totaling 10 stations. A total of 17 monitoring stations were deployed to track rock pressure and its manifestation patterns during the initial tunnel excavation phase, as illustrated in Figure 18. Monitoring parameters included: support pressure monitoring at the working face—load and deformation monitoring of constant-resistance large-deformation anchor cables—asymmetric deformation monitoring at the tunnel surface—load monitoring of hydraulic single-cylinder props—roof separation monitoring.

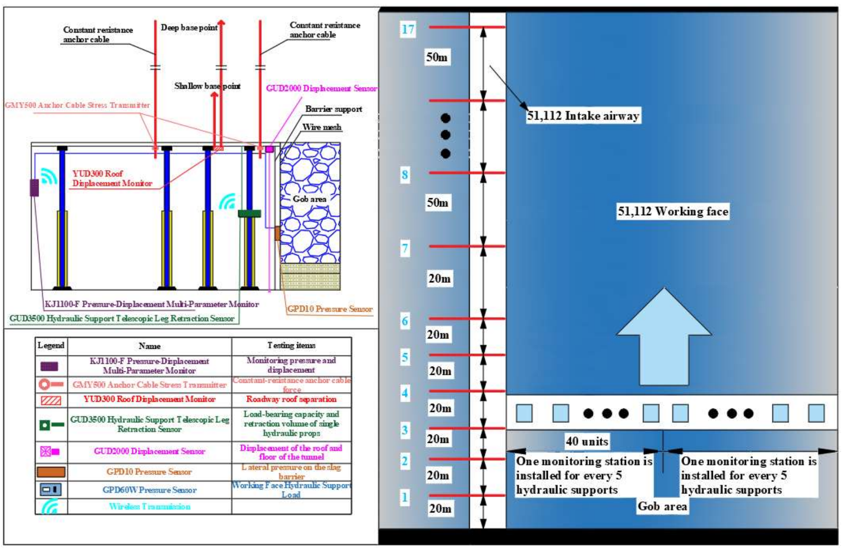

Figure 18. Schematic diagram of the monitoring station layout and monitoring content.

5.3.2. Analysis of Rock Pressure Monitoring Data

(1) Hydraulic Support Load Monitoring in the Working Face

The first column on the left of the working face rock pressure pattern cloud diagram indicates the monitoring station number, while the second column denotes the unit support number in the working face. The diagram reveals that the average pressure on the non-slitting side of the working face is 36 MPa, the average pressure in the central area is 39 MPa, and the average pressure on the slitting side is 29 MPa. Compared to the non-slitting side, the pressure on the slitting side decreased by 19.44%. Compared to the center of the working face, the pressure on the cut side decreased by 25.64%. The rock pressure distribution pattern of the working face is illustrated in Figure 19.

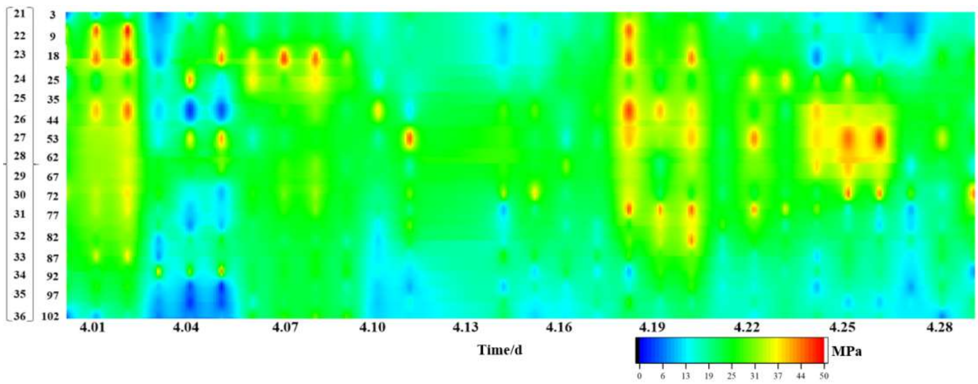

Figure 19. Analysis of mining pressure patterns at the working face.

(2) Stress Behavior of Constant-Resistance Large-Deformation Anchor Cables

Based on the advancement status of the working face and the layout of anchor cable stress gauges, stress monitoring data from constant-resistance anchor cables at the following measurement points were selected for analysis. The stress variation curve of the anchor cable located 250 m from the cut-off face is shown in Figure 20. Analysis reveals: (a) The concentrated advance stress generated by the working face advancement exerts a slight influence on anchor cable loading. The advanced influence distance of the working face is approximately 17 m, but the constant-resistance anchor cables exhibit no significant response. The primary reason is the intact and hard roof conditions, where pre-split cuts have severed part of the stress transmission, resulting in an inconspicuous advance pressure manifestation in the roadway. (b) Within the 20–80 m range behind the working face, the pressure in constant-resistance anchor cables in the retained roadway section shows a marked increase. This indicates that the old roof strata behind the working face have exerted a significant influence on the constant-resistance anchor cables. Therefore, special attention should be paid to support measures approximately 50 m behind the working face. (c) The cables at monitored stress points in the reserved roadway section have reached constant resistance. Analysis of constant-resistance cable stress trends reveals two primary patterns of stress increase: gradual increase over a distance behind the working face, and sudden increase over a distance behind the working face. Analysis of causes: for the gradual increase type, constant-resistance anchor cables are positioned between the advancing pressure and the fracture step. As the distance from the working face increases, the distance to the basic roof suspension increases, causing pressure to rise gradually. For the sudden change type, constant-resistance anchor cables are affected by advancing pressure, causing the roof rock mass to fracture and resulting in an instantaneous increase in stress.

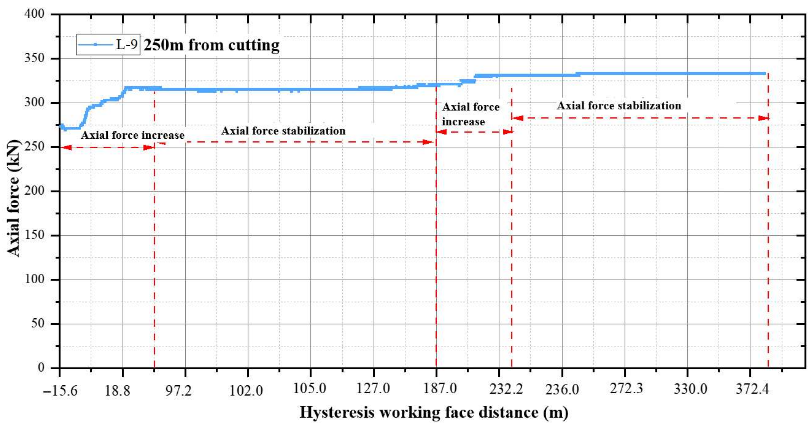

Figure 20. Stress conditions of tunnel anchors.

(3) Patterns of Roof, Floor, and Both Sides Displacement in the Roadway

To monitor surrounding rock deformation, laser distance measurement was employed to track changes in roof and floor displacement. Analysis of these displacement data yielded the following conclusions: when the trailing working face distance ranges between 100 and 180 m, surrounding rock deformation increases rapidly. The average roof and floor displacement eventually stabilizes at 300 mm, while the sidewall displacement generally remains below 40 mm. Details are shown in Figure 21.

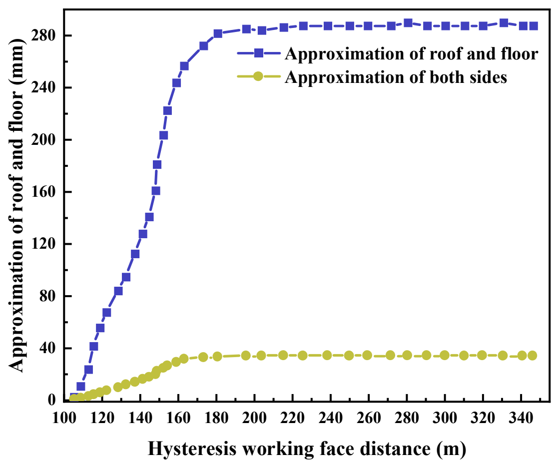

Figure 21. Surrounding rock deformation.

5.4. Study on the Manifestation Patterns of Mine Pressure During Reuse of Retained Roadways

To understand the stress variation patterns in the surrounding rock during the secondary reuse of self-formed roadways, mine pressure monitoring was conducted in the advance section of the roadway. This primarily included stress monitoring and surrounding rock deformation monitoring.

5.4.1. Analysis of Advanced Stress Monitoring During Secondary Reuse

Real-time online monitoring of mining pressure was employed to collect field data and monitor individual rock blocks. Results are shown in Figure 22. The monitoring revealed that during the secondary reuse of the self-formed roadway, the influence zone of advance stress on the advance rock blocks extended approximately 43 m. The maximum support pressure within the roadway reached 24 MPa at a distance of 10 m from the working face. Based on the relationship between stress variation patterns and distance from the working face, the zone is divided into four regions: no significant influence zone (distance > 43 m)—slow growth zone (distance 20–40 m)—accelerated growth zone (distance 11–20 m)—stable fluctuation zone (distance 0–10 m). As the distance from the working face decreases, the coal body ahead of the face develops plastic deformation, reducing its load-bearing capacity. At this stage, the stability of the roadway roof primarily relies on the internal support measures.

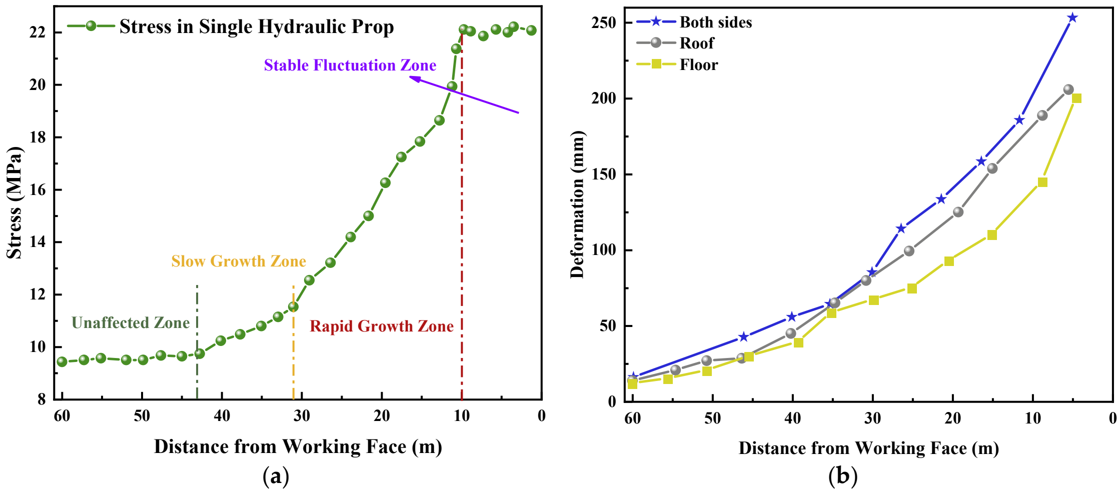

Figure 22. Rock pressure manifestation characteristics during the reuse period: (**a**) individual pressure; (**b**) rock mass deformation.

5.4.2. Monitoring of Secondary Reused Tunnel Rock Mass Deformation

During the 51,111 working face mining period, displacement of the roof and floor in the monitored tunnel sections was tracked, with results shown in Figure 22. The data indicate that during secondary reuse, the sidewall deformation was significant, followed by roof subsidence. This demonstrates that constant-resistance rock bolts effectively control roof settlement. Based on the relationship between rock mass deformation and distance from the working face, the deformation zone is divided into three regions. Slow deformation zone (>40 m from the working face): the deformation curve increases slowly, with minimal rock mass movement and a deformation rate of 3–5 mm/day. Accelerated deformation zone (10–40 m from the working face): the deformation curve increases rapidly, deformation curvature increases significantly, and rock mass movement becomes intense; Intense deformation zone (0–10 m from the working face): the deformation curve and deformation rate increase sharply, with the maximum deformation rate exceeding 40 mm/d, indicating intense rock mass movement.

5.4.3. Actual Results of Roadway Formation

The 51,112 working face commenced coal extraction in February 2023. Utilizing the roof cutting and pressure relief technology for automatic roadway formation without coal pillars, the conveyor roadway was formed automatically along the goaf. By 29 June 2023, the working face had completed extraction and successfully formed 650 m of roadway. The overall roof subsidence in the tunneling area was minimal. The maximum roof subsidence on the cutting-off side was approximately 300 mm, with an average subsidence of about 274 mm. No significant lateral bulging was observed in the rubble-filled tunnel walls, and no noticeable rib spalling occurred in the solid coal walls. These results fully meet safety and operational requirements while satisfying design specifications, demonstrating excellent application outcomes. The roadway results are illustrated in Figure 23.

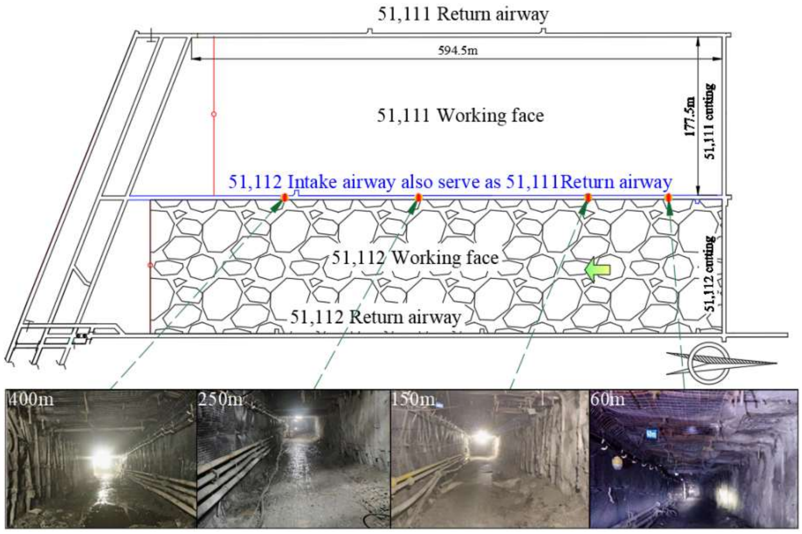

Figure 23. Actual photo of the retained roadway.

6. Discussion

The computational model simplifies infinite rock masses into finite cubes and applies non-reflective boundary conditions on the outer surfaces to simulate far-field effects. While this assumption effectively suppresses artificial reflections of stress waves, it may marginally affect the details of near-field damage distribution. Furthermore, the model does not account for geological structures (such as joints and bedding planes) or the initial anisotropy of the in situ stress field. Their influence requires correction through field calibration in practical engineering applications.

Although this coal pillar-free longwall mining technique involves increased expenditures for new constant-resistance large-deformation rock bolts and roof caving construction, it maximizes coal resource recovery, thereby yielding significant economic benefits. The pillarless longwall mining with roof caving (roof caving for self-forming roadways) technique is a “selective” technology sensitive to geological–mechanical conditions. It demonstrates significant advantages in shallow-to-medium depths, medium-hard or softer rock strata, and coal seams with simple structures, representing an efficient, economical, and environmentally friendly mining method. However, under conditions of extremely hard roof strata or deep burial with high in situ stress (accompanied by strong rheological properties), its core logic of “active roof cutting-stress transfer-rock support” faces severe challenges of “inability to cut, collapse resistance, and stability maintenance.” Technical risks and costs surge dramatically, fundamentally limiting its applicability.

7. Conclusions

This study systematically analyzed water–rock interactions, support materials, and blasting damage characteristics in roof-cutting self-forming roadway projects for shallow-buried thick coal seams. It revealed the micro-mechanisms of strength degradation in water-bearing sandstone (calcareous cement dissolution, clay mineral expansion, and pore structure deterioration). It developed a novel large-deformation anchor capable of sustaining approximately 350 kN of constant resistance within a 396–405 mm deformation range, and validated the feasibility of using shaped charge blasting to create a directional tensile stress field, thereby achieving the dual objectives of roof caving and rock mass support. Based on the dynamic response characteristics of the surrounding rock, an integrated method for longwall mining with roadway retention was proposed: “energy-focused blasting for roof cutting and pressure relief + reinforced roadway support + rock-cutting device,” along with a zoned support system (advance support zone, temporary support zone, and stable roadway section). Field application demonstrates that this technical system maintains reasonable stress distribution and controllable rock mass deformation during roadway retention, with minimal mine pressure observed during reuse phases, indicating excellent engineering applicability and stability.

Author Contributions: Y.L.: formal analysis, methodology, writing—original draft. C.L.: formal analysis, funding acquisition. Y.Z.: conceptualization, writing—review and editing, funding acquisition. Y.C.: methodology, funding acquisition. F.Z.: visualization. F.Q.: visualization. D.S.: investigation. M.W.: supervision. All authors have read and agreed to the published version of the manuscript.

Funding: This work was funded by the National Natural Science Foundation of China (No. 52374140), the National Natural Science Foundation of China for Young (No. 52404147), the Graduate Innovation Program of China University of Mining and Technology (No. 2025WLKXJ039), and the Postgraduate Research and Practice Innovation Program of Jiangsu Province (No. KYCX25_2809).

Institutional Review Board Statement: Not applicable.

Informed Consent Statement: Not applicable.

Data Availability Statement: The raw data supporting the conclusions of this article will be made available by the authors on request.

Acknowledgments: Reviewers are thanked for their insightful suggestions and comments, which improved the quality of this manuscript. And thanks to all who contributed to and funded this study.

Conflicts of Interest: Author Yitao Liu was employed by the company Ordos City Jintong Mining Industry Co., Ltd. The remaining authors declare that the research was conducted in the absence of any commercial or financial relationships that could be construed as a potential conflict of interest.

Appendix A. Derivation of Equation (3)

After simplification to a cylindrical body, the contact surface becomes relatively regular, allowing representation through simple mechanical forms. Based on the constitutive equation of the constant-resistance sleeve:

$$T = N \cdot \tan\varphi \tag{A1}$$

where

N—Constant-resistance casing pressure on the constant-resistance body, kN;
T—Frictional resistance between the constant-resistance casing and the constant-resistance body, kN;
φ—Internal friction angle between the constant-resistance casing and the constant-resistance body, kN.

From the force analysis:

$$P = 2T \tag{A2}$$

where P is constant-resistance support force, kN.

$$P = 2N \cdot \tan\varphi \tag{A3}$$

From the constitutive equation of the constant-resistance sleeve:

$$E = \frac{\sigma}{\varepsilon} \tag{A4}$$

Furthermore:

$$\sigma = \frac{N}{S_{\text{hemicylindrical body}}} \tag{A5}$$

References

1. Zhang, X.; He, M.; Yang, J.; Wang, E.; Zhang, J.; Sun, Y. An Innovative Non-Pillar Coal-Mining Technology with Automatically Formed Entry: A Case Study. *Engineering* **2020**, *6*, 1315–1329. [CrossRef]
2. Ma, X.; He, M.; Wang, J.; Gao, Y.; Zhu, D.; Liu, Y. Mine strata pressure characteristics and mechanisms in gob-side entry retention by roof cutting under medium-thick coal seam and compound roof conditions. *Energies* **2018**, *11*, 2539. [CrossRef]
3. Xie, S.; Wu, Y.; Guo, F.; Zou, H.; Chen, D.; Zhang, X.; Ma, X.; Liu, R.; Wu, C. Application of presplitting and roof-cutting control technology in coal mining: A review of technology. *Energies* **2022**, *15*, 6489. [CrossRef]
4. Huang, X.; Zhang, C.; Ren, Z. Parameter Determination and Effect Evaluation of Gob-Side Entry Retaining by Directional Roof Cutting and Pressure Releasing. *Eng. Fail. Anal.* **2024**, *156*, 107847. [CrossRef]
5. Li, J.; Yan, B.; Dong, J.; Qiang, X.; Chen, C.; Zhou, G.; Zheng, Y. Analysis of Main Roof Mechanical State in Inclined Coal Seams with Roof Cutting and Gob-Side Entry Retaining. *Symmetry* **2025**, *17*, 723. [CrossRef]
6. Yang, G.; Yang, X.; He, M.; Zhang, J.; Wang, H.; Shi, Z.; Yang, F.; Hou, S. Experimental and numerical investigations of goaf roof failure and bulking characteristics based on gob-side entry retaining by roof cutting. *Eng. Fail. Anal.* **2024**, *158*, 108000. [CrossRef]
7. Wang, H.; Jiang, J.; Wang, J.; Liu, P.; Wang, R.; Wang, J.; Hou, S.; He, M.; Ma, L. Experiment research on the control method of automatically retained entry by roof cutting pressure relief within thick hard main roof longwall top coal caving panel. *Eng. Fail. Anal.* **2025**, *168*, 109085. [CrossRef]
8. Xu, X.; Zhou, Y.; Yang, J.; Gao, Y.; Zhu, C.; Wang, Y.; Fu, Q. A new method of mining pressure control for roof cutting in advance working face. *Eng. Fail. Anal.* **2024**, *161*, 108302. [CrossRef]
9. Yang, G.; Yang, X.; Huang, R.; Kang, X.; Zhang, J.; Hou, S.; Zhou, P.; He, M. Failure mechanism and bulking characteristic of goaf roof in no-pillar mining by roof cutting technology. *Eng. Fail. Anal.* **2023**, *150*, 107320. [CrossRef]
10. Yang, G.; Yang, X.; Zhang, J.; He, M.; Hao, Z.; Yang, F.; Shao, L. Effect of roof cutting technology on broken roof rock bulking and abutment stress distribution: A physical model test. *Rock. Mech. Rock. Eng.* **2024**, *57*, 3767–3785. [CrossRef]
11. Zhang, D.; Song, D.; Zhang, L.; Luo, B. Mechanical Behavior and Stress Mechanism of Roof Cutting Gob-Side Entry Retaining in Medium-Thick Coal Seams. *Processes* **2025**, *13*, 2649. [CrossRef]
12. Lang, D.; Chen, S.; Yuan, H.; Yu, J.; Yu, Y.; Luo, S.; Hu, B.; Xie, P. Study of Reasonable Roof Cutting Parameters of Dense-Drilling Roof Cutting and Pressure Relief Self-Forming Roadway in Non-Pillar Mining. *Appl. Sci.* **2025**, *15*, 2685. [CrossRef]
13. Hu, B.; Wu, Y.; Yu, Y.; Xie, P.; Wen, H.; Zhang, H. Numerical study on the dynamic pressure control for self-forming roadways using CHRCT in thin coal seams with thick and hard roofs. *Energy Explor. Exploit.* **2024**, *42*, 2331–2350. [CrossRef]
14. Liu, S.; Li, X.; Zhu, W.; Fu, M.; Zhang, D.; Peng, B. Roof cutting mechanism of dense drilling in gob-side entry retaining and determination method of key parameters. *Coal Sci. Technol.* **2024**, *52*, 23–33.
15. Guo, S.; He, M.; Jeon, S. Visualization test and numerical simulations of 2D blasting crack propagation. *J. Rock. Mech. Geotech. Eng.* **2024**, *17*, 4871–4888. [CrossRef]
16. Wang, X.; Zhu, Y.; Wang, P.; Ren, H.; Li, P.; He, X.; Lv, J. Large Section of Soft Rock Gob-Side Entry Retaining Surrounding Rock Control. *Adv. Civ. Eng.* **2024**, *2024*, 9942330. [CrossRef]
17. Zhang, J.; He, M.; Wang, Y.; Li, H.; Yang, F.; Liu, X. Mechanism of roof cutting self-forming roadway and failure laws of overlying strata in extremely thin coal seams. *Eng. Fail. Anal.* **2026**, *185*, 110426. [CrossRef]
18. Wang, Q.; Jiang, Z.; Jiang, B.; He, M.; Yang, J.; Xue, H. Ground control method of using roof cutting pressure release and energy-absorbing reinforcement for roadway with extra-thick hard roof. *Rock. Mech. Rock. Eng.* **2023**, *56*, 7197–7215. [CrossRef]
19. Sun, X.; Qi, Z.; Zhang, Y.; Li, Z.; Xie, C.; Yang, J.; Ding, J.; He, L. Characteristics and control measures of deep and shallow dense drilling in roadway for pressure relieving by cutting roof. *Min. Metall. Explor.* **2024**, *41*, 787–803. [CrossRef]
20. Yang, S.; Li, Q.; Yue, H.; Yang, S.; Liu, F. Study on coal wall spalling characteristics and stability control of steeply inclined coal seam mining face. *Comput. Part. Mech.* **2025**, *12*, 1729–1750. [CrossRef]
21. Wu, W.; Wang, T.; Bai, J.; Liu, J.; Wang, X.; Xu, H.; Feng, G. Failure characteristics and cooperative control strategies for gob-side entry driving near an advancing working face: A case study. *Processes* **2024**, *12*, 1398. [CrossRef]
22. Cao, C.; Xie, Z.; Zhang, N.; Han, C.; Yan, G.; Mu, F.; Zhang, W. Differential roof cutting for roadway support in dual gob-side entry retention on a single working face− Multilevel continuous anchor-grouting control technology: A case study. *Eng. Fail. Anal.* **2024**, *163*, 108475. [CrossRef]
23. Zhang, J.; He, M.; Shimada, H.; Wang, Y.; Hou, S.; Liu, B.; Yang, G.; Zhou, P.; Li, H.; Wu, X. Similar model study on the principle of balanced mining and overlying strata movement law in shallow and thin coal seam based on N00 mining method. *Eng. Fail. Anal.* **2023**, *152*, 107457. [CrossRef]
24. Zhang, J.; He, M.; Yang, G.; Wang, Y.; Hou, S. N00 method with double-sided roof cutting for protecting roadways and Surface Strata. *Rock. Mech. Rock. Eng.* **2024**, *57*, 1629–1651. [CrossRef]
25. Ma, J.; Li, X.; Yao, Q.; Xia, Z.; Xu, Q.; Shan, C.; Sidorenko, A.; Aparin, A. Numerical simulation on mechanisms of dense drilling for weakening roofs and its application in roof control. *J. Cent. South. Univ.* **2023**, *30*, 1865–1886. [CrossRef]

26. Wang, Q.; Wei, H.; Jiang, B.; Wang, X.; Sun, L.; He, M. High pre-tension reinforcing technology and design for ultra-shallow buried large-span urban tunnels. *Int. J. Rock. Mech. Min. Sci.* **2024**, *182*, 105891. [CrossRef]
27. Chai, Y.; Wang, M.; Meng, L.; Wang, C.; Liang, Z.; Yang, Y.; Liu, J. Influence of roof cutting depth on stability of gob side entry in thick coal seams with a bulky limestone roof. *Sci. Rep.* **2025**, *15*, 31267. [CrossRef]
28. Liang, S.; Zhang, L.; Ge, D.; Wang, Q. Study on pressure relief effect and rock failure characteristics with different borehole diameters. *Shock Vib.* **2021**, *2021*, 3565344. [CrossRef]
29. Gai, Q.; He, M.; Gao, Y.; Li, S. Mechanism of Floor Damage Reduction in Non-pillar Mining with Automatically Formed Roadway: A Model Test Study. *Rock Mech. Rock Eng.* **2025**, *58*, 9573–9600. [CrossRef]
30. Zhang, Y.; Zhang, W.; Wang, K.; Xie, K.; Song, K.; Wang, Y. Hydromechanical properties and engineering applications of weakly cemented soft rock in jurassic strata. *ACS Omega* **2023**, *8*, 16373–16383. [CrossRef]
31. Xie, H.; Yao, Q.; Zhang, Z.; Shan, C.; Gao, H.; Yu, L.; Li, Y.; Li, X. Pore structure characterization measurement and damage assessment of coal rock under dry-wet cycling for underground water reservoirs. *Measurement* **2025**, *246*, 116739. [CrossRef]